Published in final edited form as:

Dev Biol. 2020 December 01; 468(1-2): 1–13. doi:10.1016/j.ydbio.2020.09.005.

Mouse models to study the pathophysiology of combined methylmalonic acidemia and homocystinuria, cblC type

Tiffany Chern[1,2,5], **Annita Achilleos**[1,5], **Xuefei Tong**[1], **Chih-Wei Hsu**[1], **Leeyean Wong**[1], **Ross A. Poché**[1,2,3,4,*]

[1]Department of Molecular Physiology and Biophysics, Baylor College of Medicine, Houston, TX 77030, USA.

[2]Graduate Program in Molecular Physiology and Biophysics, Baylor College of Medicine, Houston, TX 77030, USA.

[3]Development, Disease Models and Therapeutics Graduate Program, Baylor College of Medicine, Houston, TX 77030, USA.

[4]Genetics and Genomics Graduate Program, Baylor College of Medicine, Houston, TX 77030, USA.

[5]These authors contributed equally.

Abstract

Combined methylmalonic acidemia and homocystinuria, cblC type, is the most common inherited disorder of cobalamin metabolism and is characterized by severe fetal developmental defects primarily impacting the central nervous system, hematopoietic system, and heart. CblC was previously shown to be due to mutations in the *MMACHC* gene, which encodes a protein thought to function in intracellular cobalamin trafficking and biosynthesis of adenosylcobalamin (AdoCbl) and methylcobalamin (MeCbl). These coenzymes are required for the production of succinyl-CoA and methionine, respectively. However, it is currently unclear whether additional roles for MMACHC exist outside of cobalamin metabolism. Furthermore, due to a lack of sufficient animal models, the exact pathophysiology of cblC remains unknown. Here, we report the generation and characterization of two new mouse models to study the role of MMACHC *in vivo*. CRISPR/Cas9 genome editing was used to develop an *Mmachc* floxed allele *(*$Mmachc^{flox/flox}$*)*, which we validated as a conditional null. For a gain-of-function approach, we generated a transgenic mouse line that over-expresses functional *Mmachc* (*Mmachc-*$OE^{+/tg}$) capable of rescuing *Mmachc* homozygous mutant lethality. Surprisingly, our data also suggest that these mice may exhibit a partially penetrant maternal-effect rescue, which might have implications for *in utero* therapeutic interventions to treat cblC. Both the $Mmachc^{flox/flox}$ and *Mmachc-*$OE^{+/tg}$ mouse models will be valuable resources for understanding the biological roles of MMACHC in a variety of tissue contexts and allow for deeper understanding of the pathophysiology of cblC.

[*]**Correspondence:** poche@bcm.edu.

INTRODUCTION

Dietary cobalamin (vitamin B_{12}) is required for proper intermediate metabolism within the human body. Specifically, adenosylcobalamin (AdoCbl) and methylcobalamin (MeCbl) serve as essential coenzymes for methylmalonyl-CoA mutase (Muto et al.) and methionine synthase (MTR), respectively (Kolhouse and Allen 1977; Mellman et al. 1977) (Figure 1). The mitochondrial enzyme MUT functions to convert methylmalonyl-CoA, derived from branched-chain amino acid and odd-chain fatty acid catabolism, to succinyl-CoA, which is an important intermediate of the citric acid cycle (tricarboxylic acid cycle, or TCA cycle). The cytoplasmic enzyme MTR catalyzes the methylation of homocysteine (Hcy) to form the essential amino acid methionine (Froese et al. 2019) (Figure 1). The availability of AdoCbl and MeCbl to their respective enzymes is dependent on a series of essential intracellular trafficking events which convert free cobalamin intermediates into the required forms (Banerjee et al. 2009). As a result, human mutations in genes encoding components of this intracellular pathway result in a variety of inborn errors of cobalamin metabolism that are classified into 10 genetic complementation groups (cblA-G, cblJ, cblX, and mut) (Watkins and Rosenblatt 2013).

First identified in 1969, combined methylmalonic acidemia and homocystinuria, cblC type is the most common of these disorders (Mudd et al. 1969; Levy et al. 1970; Weisfeld-Adams et al. 2010). In its early onset form, infants affected with cblC often present with intrauterine growth restriction, failure to thrive, microcephaly, hydrocephalus, hypotonia, heart structural defects, mild craniofacial dysmorphia, hemolytic uremic syndrome, retinopathy, and other conditions. It was eventually discovered that the cblC phenotype is due to homozygous recessive or compound heterozygous mutations in the gene *Methylmalonic Aciduria type C and Homocystinuria (MMACHC)* (Lerner-Ellis et al. 2006). *MMACHC* encodes a protein thought to be a cobalamin-processing enzyme that is required for both the trafficking of free cobalamin within the cytoplasm as well as the decyanation and dealkylation of cobalamin derivatives leading to the production of active AdoCbl and MeCbl co-enzyme forms (Kim et al. 2008; Hannibal et al. 2009; Koutmos et al. 2011; Froese et al. 2012; Froese et al. 2015) (Figure 1). It is well-established that mutations in MMACHC result in reduced AdoCbl and MeCbl production and the consequential decrease in MUT and MTR activity. This metabolic deficiency in turn leads to the buildup of the upstream metabolites methylmalonic acid (MMA) and Hcy, and a decrease in methionine production (Lerner-Ellis et al. 2006). However, it is not clear how, when, and to what extent during development these metabolic perturbations impact the various organ systems affected in cblC. Levels of MMA are usually lower in cblC patients versus those with classical methylmalonic aciduria thereby making its contribution to disease less defined (Fowler et al. 2008). Nevertheless, there are reports that severely elevated MMA impairs mitochondrial oxidative metabolism in central nervous system (CNS) neurons and may also be excitotoxic (Okun et al. 2002; Kolker et al. 2008; Chandler et al. 2009). The connection between elevated Hcy and CNS pathophysiology is somewhat more defined and is a risk factor for a number of neurodegenerative diseases such as Alzheimer's disease, Parkinson's disease, and dementia (Obeid and Herrmann 2006). Hcy is an endogenous agonist of the *N*-methyl-D-aspartate (NMDA) receptor and its increase is

thought to result neuron excitotoxicity and oxidative injury that significantly contributes to CNS pathology (Olney et al. 1987; Kim and Pae 1996; Lipton et al. 1997).

Methionine is an essential amino acid required for the synthesis of nucleic acids, and neurotransmitters and phospholipids. It is also an important source of methyl donors for the methylation reactions which regulate gene expression (DNA methylation) and modify protein function. Thus, the decrease in methionine production observed in cblC likely results in the disruption of a variety of cellular processes. However, the specific impact of methionine reduction in the different tissues affected in cblC remains undefined. For example, several observed prenatal features of cblC, such as the cardiac structural defects, have not been found in fetuses with cystathionine beta synthase (CBS) deficiency (elevated Hcy) or isolated methylmalonic acidemia (elevated MMA). Thus, these defects are likely not due to the elevation of these metabolites, but possibly related to a methionine deficiency (Carrillo-Carrasco and Venditti 2012). The highly dynamic changes in gene expression during embryogenesis, driven by DNA and histone methylation status, may be particularly sensitive to reductions in methionine. However, disruption in the expression of specific genes and/or epigenetic regulation, and its role in the etiology of cblC, has not been studied *in vivo*.

Finally, is possible that MMACHC has other unknown biological functions in addition to cobalamin metabolism. For example, most patients with infantile cblC disease exhibit maculopathy and progressive retinal degeneration that, with the exception of cblD, is not observed in the other cbl genetic complementation groups (Schimel and Mets 2006; Gerth et al. 2008; Carrillo-Carrasco and Venditti 2012; Aleman et al. 2015; Brooks et al. 2016; Abu-El-Haija et al. 2019). It is also important to note that the protein product of the *MMADHC* gene responsible for cblD was previously shown to physically interact with MMACHC (Plesa et al. 2011; Froese et al. 2015). Therefore, it is possible that MMACHC and MMADHC together mediate biological processes unrelated to cobalamin metabolism. In the case of the mild craniofacial dysmorphia observed in cblC, there is clinical evidence suggesting that buildup of Hcy is not responsible (Shaw et al. 2009). This is further supported by morpholino knockdowns of the transcription co-factor *hcfc1b* in zebrafish, which results in loss of *mmachc* expression and severe craniofacial developmental defects, but no changes in MMA and Hcy levels (Quintana et al. 2014).

Clearly, the pathophysiology of cblC is incredibly complex and the precise role of MMACHC during development remains unclear. This problem is largely due to a lack of suitable animal models to study MMACHC function *in vivo*. Here we report the generation and characterization of two new mouse models for both loss- and gain-of-function studies. The *Mmachc*$^{flox/flox}$ line will be useful for performing tissue-specific conditional knockouts so that we may better understand the function of MMACHC in tissues, such as the retina, where its role is completely unknown. The *Mmachc-OE*$^{+/tg}$ mouse will allow researchers to assess the consequence of *Mmachc* over-expression and provide insight into its potential function outside of cobalamin metabolism. Additionally, this line will be useful for determining whether genetic modulation of the pathways downstream of MMACHC impacts other pathologies associated with increased Hcy such as neurodegenerative diseases (Obeid and Herrmann 2006).

RESULTS AND DISCUSSION

Mmachc germline mutant mice exhibit developmental defects and embryonic lethality

Currently, there are two available targeted alleles of *Mmachc*. The first described allele *($Mmachc^{GT}$)* contains a gene-trap inserted into intron 1 and is predicted to result in a nonfunctional, truncated protein containing the first 27 of 279 amino acids (Moreno-Garcia et al. 2014) (Supplemental Figure 1A-B). $Mmachc^{+/GT}$ intercrosses failed to produce viable $Mmachc^{GT/GT}$ mice at weaning and the authors went on to show that the homozygotes die at preimplantation stages between E3.5 and E5.5. The source of embryonic lethality was interpreted as being due to compromised trophectoderm development (Moreno-Garcia et al. 2014). However, this conclusion was not supported by trophectoderm-specific knockout of *Mmachc* and the biological requirement for *Mmachc* during early embryogenesis remains undefined.

The second targeted allele is $Mmachc^{tm1.1}$, which was generated by the North American Conditional Mouse Mutagenesis Project (NorCOMM) and is reported to contain a lacZ cassette insertion in place of exons 3 and 4 (Figure 2A). This allele is predicted to result in a truncated protein containing the first 92 of 279 amino acids (Supplemental Figure 1C). We obtained $Mmachc^{+/tm1.1}$ mice from NorCOMM (generated on a C57BL/6NCrl background) and performed intercrosses. Out of 6 litters, we never recovered $Mmachc^{tm1.1/tm1.1}$ weanlings (Figure 2B). Next, timed matings were used to determine whether embryonic lethality occurs. In contrast to the preimplantation lethality reported for the $Mmachc^{GT/GT}$ mice (Moreno-Garcia et al. 2014), preliminary reports from the International Mouse Phenotyping Consortium (IMPC) suggested that $Mmachc^{tm1.1/tm1.1}$ death occurs around E15.5. However, out of 25 E15.5 embryos, we recovered only 1 (4% total) $Mmachc^{tm1.1/tm1.1}$. We next attempted to recover homozygotes at E14.5 and, out of 42 embryos total, we recovered only 4 (9.5% total) that were $Mmachc^{tm1.1/tm1.1}$ (Figure 2C). Considering the low recovery of E14.5-E15.5 embryos, we next dissected E9.5 litters and found $Mmachc^{tm1.1/tm1.1}$ embryos at Mendelian ratios (Figure 2D). 7/8 E9.5 homozygous mutant embryos had yet to undergo turning and all were significantly smaller than littermates (Figure 2E). To verify that exons 3 and 4 are indeed deleted in $Mmachc^{tm1.1/tm1.1}$ mice, we extracted genomic DNA from the embryos and performed PCR using primers flanking all 4 *Mmachc* exons (Figure 2F).

In total, these data led us to conclude that the majority of $Mmachc^{tm1.1/tm1.1}$ mice die after E9.5 but before E15.5, which is later than reported for the $Mmachc^{GT/GT}$ mice (Moreno-Garcia et al. 2014). It is also important to note that, while the *Mmachc tm1.1* allele encodes 65 additional amino acids versus the *Mmachc GT* allele (Supplemental Figure 1B-C), we have no evidence that it functions as a hypomorph. Therefore, a partially functional protein is unlikely to explain the difference in the timing of embryonic lethality. It is more plausible that a genetic modifier allele or alleles are responsible for the observation of postimplantation $Mmachc^{tm1.1/tm1.1}$ escapers as this line was maintained on a C57BL/6NCrl background whereas $Mmachc^{GT/GT}$ mice were on a C57BL/6J/129SvEv and C57BL/6J/129SvEv/CD1 mixed background (Moreno-Garcia et al. 2014). Interestingly, when FVB/N was crossed into a C57BL/6J/129SvEv background, a small fraction of $Mut^{-/-}$ mice escaped

neonatal lethality with several living into adult stages (Chandler et al. 2009). Since MMACHC deficiency clearly results in obligate MUT dysfunction, it is plausible that a genetic modifier effect on *Mut* may be responsible for the *Mmachc*$^{tm1.1/tm1.1}$ escapers.

Despite the low incidence of E14.5-E15.5 *Mmachc*$^{tm1.1/tm1.1}$ mutants, we observed several interesting phenotypes. Mutants and controls were isolated, and we performed micro–computed tomography (micro-CT) of the entire embryonic volumes. In addition to their smaller size, which is consistent with intrauterine growth restriction, typically observed in early onset cblC (Carrillo-Carrasco and Venditti 2012), 2/4 *Mmachc*$^{tm1.1/tm1.1}$ embryos exhibited severe craniofacial dysmorphia including facial clefting (Figure 3A) and failure of palate fusion (Figure 3B). 4/4 mutants showed severe microphthalmia or anophthalmia (Figure 3C **and data not shown)**. Regarding CNS development, 1/4 *Mmachc*$^{tm1.1/tm1.1}$ embryos had exencephaly and 4/4 had a wavy spinal cord, which are frequently observed in mutants with neural tube defects (NTDs) (Figure 3D-F, **arrows)** (Huang et al. 2002; Stiefel et al. 2003; Ting et al. 2003; Wilson et al. 2009; Patterson et al. 2014). Importantly, NTDs are frequently observed in mouse mutants for folate one-carbon metabolism (FOCM) pathway genes, and human polymorphisms have been found to confer increased risk to NTDs (Ducker and Rabinowitz 2017; Steele et al. 2020). FOCM is directly linked to MMACHC via methylene tetrahydrofolate reductase (MTHFR), which mediates methyl group transfer (5-methyl-tetrahydrofolate or Me-H4-folate) from the folate cycle to the methionine cycle. Here, Me-H4-folate is consumed by MTR to synthesize methionine from homocysteine (Figure 1B). Disruptions in MTR activity, such as in cblC, result in a block of the methylation cycle thereby trapping 5-methyl-tetrahydrofolate, which in turn results in a suppression of the folate cycle – the so-called “methyl trap” (Scott 1999). Therefore, it is possible that some aspects of *Mmachc* mutant phenotypes, such as NTDs, are due to a secondary impact on folate metabolism. However, a recent study suggests that this relationship may be more complex than originally thought (Leung et al. 2017). Direct comparisons with *Mmachc* mutant NTDs may provide further clarification. Finally, considering that *Mmachc*$^{tm1.1/tm1.1}$ lethality occurs after E9.5, we wondered whether the mutants might suffer from severe defects in heart development. Indeed, micro-CT revealed 4/4 E14.5 homozygous mutants with thin, hypertrabeculated ventricles and ventricular septum defects (Figure 3G, **arrowhead and arrows)**.

All of the above-mentioned phenotypes could be interpreted as a severe form of cblC affecting craniofacial, eye, spinal cord, brain, and heart development. Specifically, cblC patients are reported to suffer from a variety of mild dysmorphic craniofacial features including long facies, flat philtrum and large low-set ears, broad nasal bridge, and tooth enamel hypoplasia (Cerone et al. 1999; Bassim et al. 2009; D'Alessandro et al. 2010). Also, maculopathy and progressive retinal dysfunction/degeneration are seen in most cblC patients (Schimel and Mets 2006; Gerth et al. 2008; Carrillo-Carrasco and Venditti 2012; Aleman et al. 2015; Brooks et al. 2016). CblC also results in a wide range of CNS developmental disorders such as microcephaly, hydrocephalus, cognitive deficiency, hypotonia, and seizures. Congenital heart defects (CHDs) including fetal dilated cardiomyopathy, ventricular hypertrabeculation, and atrial or ventricular septum defects, have also been reported (Tomaske et al. 2001; De Bie et al. 2009; Profitlich et al. 2009; Tanpaiboon et al.

2013). For all of these diverse phenotypes, the cellular origin remains mostly unknown. For example, it is possible that the retinal degeneration observed in cblC patients is due to defects in the retinal pigment epithelium or in retinal neurons. It is also possible that the degeneration is a secondary consequence of defects in retinal progenitor cell proliferation or differentiation earlier in development. Due to the phenotypic pleiotropy, severity, and lethality of the *Mmachc*$^{GT/GT}$ and *Mmachc*$^{tm1.1/tm1.1}$ mice, answering such questions requires a conditional knockout approach.

Generation and characterization of the *Mmachc* floxed allele.

We used CRISPR/Cas9 gene editing to flank *Mmachc* exons 2-4 with loxP sites (Figure 4A). We performed pronuclear injections on C57BL/6J zygotes and obtained 33 viable pups of which 6 revealed homozygous targeting of the *Mmachc* locus. From two of these pups, we established independent inbred founder lines by crossing to C57BL/6J mice (Figure 4B-C). Founder #1's line was selected for expansion and further characterization. We verified that *Mmachc*$^{flox/flox}$ mice are born at normal Mendelian ratios, are viable and fertile, and exhibit no overt phenotype (Figure 4D-E **and data not shown)**. To verify Cre mediated deletion of exons 2-4, *Mmachc*$^{flox/flox}$ mice were crossed to *E2A-Cre*$^{+/tg}$ germline deleter mice (Lakso et al. 1996). The resulting *E2A-Cre*$^{+/tg}$*; Mmachc*$^{+/flox}$ offspring were then crossed to wild-type C57BL/6J and the progeny genotyped for deletion of *Mmachc* exons 2-4 *(Mmachc*$^{+/\Delta}$) (Figure 4F-G). We next performed intercrosses of identified *Mmachc*$^{+/\Delta}$ mice to assess for Mendelian inheritance and we failed to recover any *Mmachc*$^{\Delta/\Delta}$ progeny at weaning suggesting embryonic lethality as was observed for the *Mmachc*$^{GT/GT}$ and *Mmachc*$^{tm1.1/tm1.1}$ mice (Figure 5A).

To determine when *Mmachc*$^{\Delta/\Delta}$ mice die *in utero*, timed heterozygous matings were performed. Like the *tm1.1* allele, we identified only 1/28 (3.6% total) *Mmachc*$^{\Delta/\Delta}$ embryos at E15.5 whereas E9.5 embryos were present at Mendelian ratios (Figure 5B-C). These data suggest that the *Mmachc*$^{\Delta/\Delta}$ embryos die between E9.5 and E15.5. The single E15.5 *Mmachc*$^{\Delta/\Delta}$ embryo was smaller, anophthalmic, and exhibited craniofacial dysmorphia similar to the *Mmachc*$^{tm1.1/tm1.1}$ mice (Figure 5D, **and data not shown)**. At E9.5, *Mmachc*$^{\Delta/\Delta}$ embryos had heartbeats but, like the *Mmachc*$^{tm1.1/tm1.1}$ embryos, had yet to undergo turning (Figure 5E). Interestingly, the single recovered E15.5 *Mmachc*$^{\Delta/\Delta}$ embryo showed what appeared to be right ventricular hypoplasia raising the possibility that a heart defect causes embryonic lethality (Figure 5F, **arrow)**. From these data, we conclude that the similarities between the *Mmachc*$^{\Delta/\Delta}$ and *Mmachc*$^{tm1.1/tm1.1}$ phenotypes and time of death support the idea that *tm1.1* is a null allele and not hypomorphic. However, the discrepancy with the preimplantation lethality of the *Mmachc*$^{GT/GT}$ mutants remains unresolved but may relate to genetic background-specific modifiers. Since the *Mmachc*$^{+/\Delta}$ and *Mmachc*$^{+/tm1.1}$ mice are viable, fertile, have no overt phenotype, and normal levels of MMA and Hcy, we also conclude that these alleles are not haploinsufficient (Figure 5G-I).

Generation and characterization of the *Mmachc-OE* transgenic mice.

To study MMACHC through a gain-of-function approach, we generated a transgenic mouse line aimed at ubiquitous over-expression of *Mmachc (Mmachc-OE*$^{+/tg}$). We cloned a DNA construct containing a *CAG* (cytomegalovirus/β-actin) enhancer-promoter (Miyazaki et al.

1989) upstream of an *Mmachc* cDNA followed by an *IRES-GFP-pA* cassette to monitor transgene expression (Figure 6A). This ~5kb DNA fragment was microinjected into single-cell C57BL/6J zygotes. Out of 27 weanlings, PCR genotyping of tail DNA indicated that we recovered 5 transgenic founder mice. To assess transgene expression by GFP fluorescence, these 5 founder mice were bred to CD1 mice (Charles River Lab) and litters imaged at E16.5. To establish transgenic lines, the 2 founders whose progeny exhibited the brightest GFP expression were bred to C57BL/6J mice (Figure 6B-D). Subsequent analyses were performed on founder line #1. We performed qrtPCR on whole E16.5 brain lysates and verified that the *Mmachc-OE*$^{+/tg}$ line indeed showed an increase in *Mmachc* expression (Figure 6E). We also performed Western blot analysis of MMACHC and GFP expression from whole E16.5 brain lysates and confirmed that the increased *Mmachc* mRNA expression corresponds to an increase in protein levels (Figure 6F). Using the retina as an example, we determined that the transgene is also expressed in adult tissues (Figure 6G-H). Finally, *Mmachc-OE*$^{+/tg}$ mice were crossed to wild-type C57BL/6J mice, and we found that the transgene is inherited in a Mendelian ratio and that *Mmachc-OE*$^{+/tg}$ mice are viable, fertile, and do not exhibit any overt phenotype (Figure 6I-J, **and data not shown)**. To verify that the *Mmachc-OE* is widely expressed in developing tissues impacted in cblC, we performed confocal analysis of E15.5 cryosections. Broad GFP expression was observed in the developing retina, cerebral cortex, spinal cord, heart, craniofacial area, and liver (Figure 7A-F). In total, these data indicate that widespread over-expression of MMACHC during development has no obvious deleterious consequence. These data also raise the possibility that most, if not all, tissues can tolerate exogenous *Mmachc* expression. This finding is important as there are several current efforts using viral-mediated gene replacement therapies to treat other methylmalonic acidemias (Chandler and Venditti 2008; Chandler and Venditti 2010; Chandler and Venditti 2019). Therefore, a similar approach may be possible for cblC.

Assessment of *Mmachc-OE* transgene functionality

Despite the widespread over-expression of the *Mmachc-OE* transgene *in vivo*, it is possible that the transgenic MMACHC protein may not be functionally equivalent to endogenous MMACHC. Therefore, we crossed the *Mmachc-OE* transgene onto the *Mmachc*$^{tm1.1/tm1.1}$ homozygous mutant background and assessed litters for phenotypic rescue. *Mmachc*$^{+/tm1.1}$; *Mmachc-OE*+/^{tg} males were bred to *Mmachc*$^{+/tm1.1}$ females. At weaning, the resulting litters were genotyped, and we recovered *Mmachc*$^{tm1.1/tm1.1}$; *Mmachc-OE*$^{+/tg}$ mice at normal Mendelian ratios whereas *Mmachc*$^{tm1.1/tm1.1}$ mice, not carrying the transgene, were not present (Figure 8A-B). The rescue of *Mmachc*$^{tm1.1/tm1.1}$ embryonic lethality suggests that the transgene encoded MMACHC is biologically functional. It is also worth noting that these mice did not exhibit any gross craniofacial, ocular, or neurological abnormalities, and were fertile (Figure 8B, **arrowheads and data not shown)**. However, we did notice that the rescued *Mmachc*$^{tm1.1/tm1.1}$; *Mmachc-OE*$^{+/tg}$ weanlings were on average 30% smaller than the controls and remained so throughout adulthood (Figure 8C). These data indicate that the *Mmachc-OE* transgene, while functional, is not 100% equivalent to endogenous *Mmachc*. This result is likely due to key differences in spatial and temporal transgene expression. It is also possible that *Mmachc*$^{tm1.1/tm1.1}$; *Mmachc-OE*$^{+/tg}$ mice are more akin to a weak hypomorphic allele of *Mmachc*. Such a mouse might bypass embryonic lethality, yet

recapitulate some aspects of human cblC symptoms, such as the metabolic perturbations, and serve as a new and valuable animal model of this disease. Consistent with this idea, we found that *Mmachc*$^{tm1.1/tm1.1}$; *Mmachc-OE*$^{+/tg}$ adult mice had tremendously elevated levels of MMA and Hcy in their plasma (Figure 8D). In the future, it will be important to define the molecular basis of this partial rescue and determine whether the increase in MMA and Hcy impacts CNS physiology.

Finally, it is worth noting that, when we crossed *Mmachc*$^{+/tm1.1}$ males to *Mmachc*$^{+/tm1.1}$; *Mmachc-OE*$^{+/tg}$ females, we surprisingly recovered 2 viable *Mmachc*$^{tm1.1/tm1.1}$ mice that did not carry the transgene (Figure 8E). Analogous to the *Mmachc*$^{tm1.1/tm1.1}$; *Mmachc-OE* $^{+/tg}$ mice, these mice were smaller than their littermates and, with the exception of being infertile, did not exhibit any gross defects by 8 weeks of age. However, it should be noted that we have not yet recovered enough maternal-effect rescued mice to determine the long-term consequence of not having functional MMACHC as these mice age. From the same cross, we also recovered 1 *Mmachc*$^{tm1.1/tm1.1}$ mouse at postnatal day 0, which was never recovered from *Mmachc*$^{+/tm1.1}$ intercrosses. This pup still suffered from facial clefting and anophthalmia and did not survive postnatally (Figure 8F, **arrows and arrowheads).**

Our data suggesting a partially penetrant, maternal-effect rescue by the *Mmachc-OE* transgene raises the intriguing possibility that a critical window of MMACHC requirement exists during embryogenesis and it can be satisfied by temporary *Mmachc* gene supplementation via the maternal environment. The origin of this maternal-effect rescue remains to be identified, but it is possible that the developing fetus may have access to the transgenic mother's elevated levels of *Mmachc* mRNA or protein or she produces large amounts of AdoCbl and MeCbl, which are available to the fetus. Consistent with this idea, zinc finger nucleases were recently used to generate the first zebrafish germline mutant alleles of *mmachc* (Sloan et al. 2020). Homozygous mutant fish exhibited cblC metabolic defects, runtedness, and lethality by 42-day post-fertilization (dpf). Interestingly, this phenotype is much less severe than *mmachc* morpholino knockdowns, which die by 6 dpf. The authors speculate that maternally derived *mmachc* mRNA in the unfertilized egg may rescue the mutant fish from early embryonic lethality.

CONCLUSIONS

We have developed and functionally validated two new mouse models that will shed greater light on the pathophysiology of cblC. The *Mmachc* floxed allele will allow for temporal- and tissue-specific knockout of *Mmachc* thereby bypassing embryonic lethality and facilitating the study of its role in a variety of contexts such as the developing heart and retina. The *Mmachc-OE* transgenic mice, along with cobalamin supplementation, will be useful for determining whether MMACHC has cobalamin-independent roles during development. For example, if the phenotype of tissue-specific knockouts of *Mmachc* is rescued by transgenic *Mmachc*, but not cobalamin treatment, this result would indicate a cobalamin-independent role. Also, by providing evidence suggesting a maternal-effect rescue of *Mmachc* mutant lethality, the *Mmachc-OE* mice have also uncovered a possible route of *Mmachc* supplementation via the maternal environment. The mechanism of this

maternal-effect rescue is currently unknown but might prove to be a promising therapeutic approach versus cobalamin supplementation alone.

METHODS

Mice

All animal research was conducted according to protocols approved by the Institutional Animal Care and Use Committee (IACUC) of Baylor College of Medicine. Since there were no age- or sex-dependent differences in our observations, male and female data were combined for presentation herein. Mouse stains used or generated, and the genotyping methods are shown in detail below. All generated mouse lines will be made available to the research community.

Mmachc tm1.1 mice and Genotyping

Mmachc$^{+/tm1.1}$ mice (C57BL/6NCrl background) were generated by the North American Conditional Mouse Mutagenesis Project and obtained from the Canadian Mouse Mutant Repository (CMMR). The following primers were used for PCR genotyping and generated 100 bp and 229 bp products for the wild-type and tm1.1 alleles, respectively: MmcWT FW 5'-ATGTTGCTGCCAGGGATTGAAGTGCC -3', MmcWT RV 5'-TGAAACCTTCAAGCAGAGTGATGCGGC-3', MmcTm1.1 F 5'ATTGGGTTCTATGCTGTCTGTGGAGCC -3', and MmcTm1.1 R 5'-CACCGACGCCAATCACAAACAC-3'. To confirm the deletion of exons 3 and 4, the following primer pairs were used to amplify the 4 exons of the *Mmachc* gene: Mex1_F 5'-GCAGAGTCAGTTGAGTCCGTT-3' and Mex1_R 5'-TTTTGGCACCAAGGCCAATC -3' (270 bp); Mex2_F 5'-ATCCAACTGCCTGAGCTTTCT-3' and Mex2_R 5'-AAGCTAGGTCAACAGGGAAGC-3 (285 bp)'; Mex3_F 5'-CTCCCATCATGCTAACAAGCG -3' and Mex3 R 5'-GGAGCCTTTACTATCCTTTCCCT-3' (251 bp); Mex4_F 5'-CCCATACTTGGGGGATAAAAAGT-3' and Mex4_R 5'-GGGGTGGATTCCTGTTCAAGG-3' (1715 bp).

Generation of *Mmachc floxed* (*MmachC*$^{flox/flox}$) mice

The *Mmachc* floxed *(Mmachc*$^{flox/flox}$*)* mouse line was generated by using CRISPR/Cas9 genome editing. LoxP sites were inserted flanking exons 2 to 4 of the *Mmachc* gene. Two single guide RNAs (sgRNAs), two single-stranded oligonucleotides (ssOligos, DNA donors), and Cas9 mRNA were purchased from Integrated DNA Technologies, Inc. and microinjected into two hundred single-cell C57BL/6J mouse zygotes by the Baylor College of Medicine Genetically Engineered Mouse Core. We obtained 33 weanlings that were PCR genotyped using the following primers: MLox_F1 5'-TCTCCTTGCTGCCATCTTGG-3' and MLox_R1 5'-TAGTAGGAGAGAGGTTGGGC-3' (to detect a 174 bp WT band and 214 bp floxed band), and MLox_F2 5'-CACCCAGGAAGGAGAGAGGT-3' and M_Lox_R2 5'-CCTACCAGTTTTCAGGATGCA-3' (to detect a 194 bp WT band and 234 bp floxed band). As indicated by a failure to amplify a wild-type band, we identified 6 putative homozygous floxed founder mice. To confirm correct targeting, we sequenced the PCR products and selected a male founder who was then backcrossed to C57BL/6J for 4 generations to

establish an inbred *Mmachc*$^{flox/flox}$ line. The *E2A-Cre*$^{+/tg}$ deleter strain (Lakso et al. 1996) was crossed to the *Mmachc*$^{flox/flox}$ line to generate the *Mmachc* deletion *(Mmachc*$^{\Delta/\Delta}$) allele. MLox_F1 and MLox_R2 primers, giving a band of 236 bp, were used to identify deletion of *Mmachc* exons 2-4. For further details on CRISPR/Cas9 targeting of *Mmachc*, please see Supplemental file 1.

Generation of *Mmachc* over-expression (*Mmachc-OE*$^{+/tg}$) mice

The open reading frame of *Mmachc* was released from the PCMV6-Kan/Neo vector (OriGene, #MC202568) by digestion with AscI and BamHI followed by blunting with T4 DNA polymerase. This ~850 bp fragment was then ligated to the pCAGIG plasmid (Addgene plasmid #11159, a gift from Connie Cepko) that was digested with EcoRV. The resulting plasmid containing the transgenic construct was then digested with SalI and BamHI and the ~5 kb *CAG-Mmachc-IRES-GFP-pA* transgene fragment was purified and microinjected into single-cell C57BL/6J mouse zygotes by the Baylor College of Medicine GEM Core. PCR genotyping of tail DNA revealed 5 positive founder mice out of 27 weanlings total. The following primers were used and generated a 914 bp product: MOE_F 5'-TCCAGGTGGCGTGGTACAAT-3' and MOE_R 5'-CACATTGCCAAAAGACGGCA-3'. The founder mice were bred to CD1 mice (Charles River Lab) for assessment of GFP fluorescence. Two lines exhibiting the brightest fluorescence were also bred to C57BL/6J mice to establish an inbred *Mmachc-OE*$^{+/tg}$ line for subsequent experiments.

To genotype the *Mmachc*$^{tm1.1/tm1.1}$*; Mmachc-OE*$^{+/tg}$ rescued mice, the following primers were used to generate 366 bp, 229 bp, and 173 bp products corresponding to the *Mmachc* wild-type allele, the tm1.1 allele, and the transgene *(Gfp),* respectively: MmcWT2 F 5'-CAGTGCTCTTCACCACTGAGC -3', MmcWT2 R 5'- ACCTGCTATGTGCTGGGGA −3', MmcTm1.1 F 5'-ATTGGGTTCTATGCTGTCTGTGGAGCC −3', and MmcTm1.1 R 5'-CACCGACGCCAATCACAAACAC-3', GFP F 5'- AAGTTCATCTGCACCACCG −3', GFP R 5'- TCCTTGAAGAAGATGGTGCG −3'.

Micro-computed tomography (micro-CT) sample preparation and scanning

E14.5 and E15.5 *Mmachc*$^{+/+}$, *Mmachc*$^{tm1.1/tm1.1}$ and *Mmachc*$^{\Delta/\Delta}$ mice were dissected in ice-cold 0.1M Phosphate Buffered Saline (PBS) and fixed in 4% paraformaldehyde (PFA) overnight at 4°C. After fixation, embryos were transferred to new tubes and immersed in fresh stabilization buffer (SB) [4% PFA, 4% acrylamide (Bio-Rad, 161-0140), 0.05% bis-acrylamide (Bio-Rad, 161-0142), 0.25% VA044 initiator (Wako Chemical, 017-19362), 0.05% Saponin (Sigma, 84510) in PBS] for 3 days at 4°C. Then, sample tubes were capped off and purged with nitrogen at 10 psi for 3 minutes. Tubes with samples were recapped and incubated for 3 hours at 37°C for the hydrogel to polymerize. Samples were removed from the hydrogel and stored in PBS with 0.1% sodium azide at 4°C until ready for imaging. Before micro-CT scanning, embryos were immersed in 0.1N iodine (Thermo Fisher, SI86-1) and rocked overnight at room temperature. Micro-CT images were acquired using a Bruker SkyScan 1272 Scanner at a 11 μm resolution in the Baylor College of Medicine Optical Imaging & Vital Microscopy (OIVM) Core.

Tissue collection, preparation and image acquisition

Whole embryos or tissues were dissected in ice-cold PBS and fixed in 4% PFA for 1 hour at 4°C. Following PBS washes (3 times for 10 minutes each), the tissue was transferred to a clean petri dish filled with PBS. Bright field images were taken using a dissection microscope connected to a camera. Imaging of GFP fluorescent was performed using a Zeiss Axio Zoom V16 Stereo/Zoom Microscope with 5X and 10X objectives.

To prepare cryosections, wild-type and *Mmachc-OE*$^{+/tg}$ embryos were fixed in 4% PFA for 1 hour at 4°C and then washed in PBS (3 times for 10 minutes each). This was followed by incubation in a 15% sucrose solution (made in PBS) overnight at 4°C, and then a 30% sucrose incubation for an additional night at 4°C. The embryos were then submerged in OCT compound (Sakura, 4583), frozen on dry ice, and cryosectioned into 50μm sections. Tissue sections were mounted on Superfrost Plus slides (VWR) and coverslips were mounted with Fluoromount-G (Southern Biotech, 0100-01) prior to confocal microscopy. Imaging of GFP fluorescence was performed using a Zeiss LSM 780 inverted confocal microscope with 20X and 40X objectives. All fluorescent microscopy imaging was done in the Baylor College of Medicine OIVM Core. For standardization between wild-type and *Mmachc-OE*$^{+/tg}$ samples, all images were acquired with the same laser power, detector gain, scan speed, and pinhole size.

Mouse plasma collection and metabolite measurements

Blood from wild-type, *Mmachc*$^{+/tm1.1}$, *Mmachc*$^{+/\Delta}$, *Mmachc*$^{+/tm1.1}$*; Mmachc-OE*$^{+/tg}$ and *Mmachc*$^{tm1.1/tm1.1}$*; Mmachc -OE*$^{+/tg}$ adult mice was collected retro-orbitally using heparinized capillary tubes (Thermo Fisher, 22-260950). The samples were then centrifuged at 4°C (10,000 RPM, 15 minutes) and the plasma was transferred to a new tube. The plasma was stored at −80°C until sent to Biochemical Genetics Laboratory at Baylor Genetics for MMA and Hcy level determination by liquid chromatography-tandem mass spectrometry (Jiang et al. 2017).

RNA extraction and quantitative rtPCR

Brains from E16.5 and retinae from adult wild-type and *Mmachc-OE*$^{+/tg}$ mice were dissected and total RNA was purified using the RNeasy Mini Kit (QIAGEN). The purified RNA was reverse transcribed using the SuperScript III first strand synthesis kit with Oligo (dT)20 and random hexamer priming (Invitrogen). QrtPCR was performed with the Taqman gene expression assay (Applied Biosystems) for *Mmachc* (Mm00482455_m1). *Gapdh* (Mm4352932), and *Beta-actin* (Mm4352933) probes were used for normalization. The conditions to perform qrtPCR using a StepOnePlus Real-Time PCR System (Life Technologies) were: 50°C for 2 minutes, 95°C for 10 minutes, 40 cycles of 95°C for 15 s and 60°C for 1 minute.

Western blot analysis

E16.5 brains were dissected from wild-type and *Mmachc-OE*$^{+/tg}$ mice in PBS and briefly washed in PBS containing protease inhibitor (Thermo Scientific, 1862209) and phosphatase inhibitor (Thermo Scientific, 78420). The PBS was removed, and the brains were flash-frozen and kept at −80°C until used. Samples were thawed on ice for 10 minutes in ice cold

lysis buffer (Thermo Scientific 1861603) containing protease and phosphatase inhibitors. Brains were homogenized and centrifuged at 4°C (2,000 RPM, 10 minutes) and the supernatant was transferred to a new tube. Cleared protein lysates were quantified by the Bradford assay. 30 or 100μg of protein was loaded onto a 4%–15% Tris/Glycine precast gels (Bio-Rad, 5671084) for electrophoresis and subsequently transferred (30V, overnight) onto Immobilon-P PVDF membranes using the Criterion™ System Bio-Rad. Membranes were washed in TBS-T pH 7.4 (20 mM Tris, 137 mM NaCl, 0.1% Tween 20) and blocked for 1 hour at RT with 5% non-fat milk solution to reduce non-specific antibody binding. Three independent wild-type and transgenic samples were probed with the following primary antibodies (in 5% milk, overnight at 4°C): MMACHC (1:1000, NeuroMabs, N230/21) and GFP (1:1000, Cell signaling, 2555S). VINCULIN (1:3000, Cell Signaling, 13901) was used as loading control. Following primary antibody incubation, membranes were washed in TBS-T, incubated with HRP-conjugated secondary antibodies (1-hour, room temperature), detected with Clarity™ Western ECL Substrate (Bio-Rad, 170–5060) and imaged with the Chemidoc Touch Imager (Bio-Rad).

Quantification and statistical analysis

For quantification of mRNA by qrtPCR, each qrtPCR reaction was performed in triplicate for each independent cDNA samples (N = 3). The mean ΔCt values of *Mmachc* were normalized against the housekeeping genes *Gapdh* or *Beta-actin* and corresponding ΔΔCt values were log2-transformed to obtain fold change values. For data analysis, the Pfaffl method was used to determine relative gene expression ratios and a p value of < 0.05 was considered significant (Pfaffl 2001).

For body weight tracking, wild-type, $Mmachc^{+/flox}$, $MmachC^{flox/flox}$, $Mmachc\text{-}OE^{+/tg}$, $Mmachc^{+/tm1.1}$; $Mmachc\text{ -}OE^{+/tg}$ and $Mmachc^{tm1.1/tm1.1}$; $Mmachc\text{ -}OE^{+/tg}$ mice were weighed at the desired age. The Student's t test was used to determine differences between groups. P values < 0.05 were considered significant.

The Pearson's chi-squared (χ^2) test was used to evaluate the fit of the observed genotype distributions within the expected Mendelian ratios. The ratios of embryonic and weanling wild-type, $Mmachc^{+/tm1.1}$, $Mmachc^{tm1.1/tm1.1}$, $Mmachc^{+/\Delta}$, $Mmachc^{\Delta/\Delta}$, and $Mmachc^{flox/flox}$ mice were calculated to obtain the deviation from the Mendelian ratios. P values < 0.05 were considered significant.

One-way ANOVA and a post hoc Tukey's test was used to determine significance in changes of plasma MMA and Hcy levels.

Supplementary Material

Refer to Web version on PubMed Central for supplementary material.

ACKNOWLEDGEMENTS

We thank the Optical Imaging and Vital Microscopy (OIVM) and Genetically Engineered Mouse Core facilities at Baylor College of Medicine, and the Baylor Genetics Biochemical Genetics Laboratory for their services. This work was supported by grants from the National Institutes of Health: R01 EY024906 and R01 DE028298 to Ross Poche and T32 EY007102 to Graeme Mardon (supporting Tiffany Chern).

REFERENCES

Abu-El-Haija A, Mendelsohn BA, Duncan JL, Moore AT, Glenn OA, Weisiger K, Gallagher RC. 2019 Cobalamin D Deficiency Identified Through Newborn Screening. JIMD Rep 44: 73–77. [PubMed: 30097992]

Aleman TS, Brodie F, Garvin C, Gewaily DY, Ficicioglu CH, Mills MD, Forbes BJ, Maguire AM, Davidson SL. 2015 Retinal Structure in Cobalamin C Disease: Mechanistic and Therapeutic Implications. Ophthalmic Genet 36: 339–348. [PubMed: 24512365]

Banerjee R, Gherasim C, Padovani D. 2009 The tinker, tailor, soldier in intracellular B12 trafficking. Curr Opin Chem Biol 13: 484–491. [PubMed: 19665918]

Bassim CW, Wright JT, Guadagnini JP, Muralidharan R, Sloan J, Domingo DL, Venditti CP, Hart TC. 2009 Enamel defects and salivary methylmalonate in methylmalonic acidemia. Oral Dis 15: 196–205. [PubMed: 19143946]

Brooks BP, Thompson AH, Sloan JL, Manoli I, Carrillo-Carrasco N, Zein WM, Venditti CP. 2016 Ophthalmic Manifestations and Long-Term Visual Outcomes in Patients with Cobalamin C Deficiency. Ophthalmology 123: 571–582. [PubMed: 26825575]

Carrillo-Carrasco N, Venditti CP. 2012 Combined methylmalonic acidemia and homocystinuria, cblC type. II. Complications, pathophysiology, and outcomes. J Inherit Metab Dis 35: 103–114. [PubMed: 21748408]

Cerone R, Schiaffino MC, Caruso U, Lupino S, Gatti R. 1999 Minor facial anomalies in combined methylmalonic aciduria and homocystinuria due to a defect in cobalamin metabolism. J Inherit Metab Dis 22: 247–250. [PubMed: 10384379]

Chandler RJ, Venditti CP. 2008 Adenovirus-mediated gene delivery rescues a neonatal lethal murine model of mut(0) methylmalonic acidemia. Hum Gene Ther 19: 53–60. [PubMed: 18052792]

-. 2010 Long-term rescue of a lethal murine model of methylmalonic acidemia using adeno-associated viral gene therapy. Mol Ther 18: 11–16. [PubMed: 19861951]

-. 2019 Gene Therapy for Methylmalonic Acidemia: Past, Present, and Future. Hum Gene Ther 30: 1236–1244. [PubMed: 31303064]

Chandler RJ, Zerfas PM, Shanske S, Sloan J, Hoffmann V, DiMauro S, Venditti CP. 2009 Mitochondrial dysfunction in mut methylmalonic acidemia. FASEB J 23: 1252–1261. [PubMed: 19088183]

D'Alessandro G, Tagariello T, Piana G. 2010 Oral and craniofacial findings in a patient with methylmalonic aciduria and homocystinuria: review and a case report. Minerva Stomatol 59: 129–137. [PubMed: 20357739]

De Bie I, Nizard SD, Mitchell GA. 2009 Fetal dilated cardiomyopathy: an unsuspected presentation of methylmalonic aciduria and hyperhomocystinuria, cblC type. Prenat Diagn 29: 266–270. [PubMed: 19248038]

Ducker GS, Rabinowitz JD. 2017 One-Carbon Metabolism in Health and Disease. Cell Metab 25: 27–42. [PubMed: 27641100]

Fowler B, Leonard JV, Baumgartner MR. 2008 Causes of and diagnostic approach to methylmalonic acidurias. J Inherit Metab Dis 31: 350–360. [PubMed: 18563633]

Froese DS, Fowler B, Baumgartner MR. 2019 Vitamin B12 , folate, and the methionine remethylation cycle-biochemistry, pathways, and regulation. J Inherit Metab Dis 42: 673–685. [PubMed: 30693532]

Froese DS, Kopec J, Fitzpatrick F, Schuller M, McCorvie TJ, Chalk R, Plessl T, Fettelschoss V, Fowler B, Baumgartner MR et al. 2015 Structural Insights into the MMACHC-MMADHC Protein Complex Involved in Vitamin B12 Trafficking. J Biol Chem 290: 29167–29177. [PubMed: 26483544]

Froese DS, Krojer T, Wu X, Shrestha R, Kiyani W, von Delft F, Gravel RA, Oppermann U, Yue WW. 2012 Structure of MMACHC reveals an arginine-rich pocket and a domain-swapped dimer for its B12 processing function. Biochemistry 51: 5083–5090. [PubMed: 22642810]

Gerth C, Morel CF, Feigenbaum A, Levin AV. 2008 Ocular phenotype in patients with methylmalonic aciduria and homocystinuria, cobalamin C type. J AAPOS 12: 591–596. [PubMed: 18848477]

Hannibal L, Kim J, Brasch NE, Wang S, Rosenblatt DS, Banerjee R, Jacobsen DW. 2009 Processing of alkylcobalamins in mammalian cells: A role for the MMACHC (cblC) gene product. Mol Genet Metab 97: 260–266. [PubMed: 19447654]

Huang Y, Roelink H, McKnight GS. 2002 Protein kinase A deficiency causes axially localized neural tube defects in mice. J Biol Chem 277: 19889–19896. [PubMed: 11886853]

Jiang Y, Mistretta B, Elsea S, Sun Q. 2017 Simultaneous determination of plasma total homocysteine and methionine by liquid chromatography-tandem mass spectrometry. Clin Chim Acta 464: 93–97. [PubMed: 27845054]

Kim J, Gherasim C, Banerjee R. 2008 Decyanation of vitamin B12 by a trafficking chaperone. Proc Natl Acad Sci U S A 105: 14551–14554. [PubMed: 18779575]

Kim WK, Pae YS. 1996 Involvement of N-methyl-d-aspartate receptor and free radical in homocysteine-mediated toxicity on rat cerebellar granule cells in culture. Neurosci Lett 216: 117–120. [PubMed: 8904797]

Kolhouse JF, Allen RH. 1977 Recognition of two intracellular cobalamin binding proteins and their identification as methylmalonyl-CoA mutase and methionine synthetase. Proc Natl Acad Sci U S A 74: 921–925. [PubMed: 15259]

Kolker S, Sauer SW, Hoffmann GF, Muller I, Morath MA, Okun JG. 2008 Pathogenesis of CNS involvement in disorders of amino and organic acid metabolism. J Inherit Metab Dis 31: 194–204. [PubMed: 18392748]

Koutmos M, Gherasim C, Smith JL, Banerjee R. 2011 Structural basis of multifunctionality in a vitamin B12-processing enzyme. J Biol Chem 286: 29780–29787. [PubMed: 21697092]

Lakso M, Pichel JG, Gorman JR, Sauer B, Okamoto Y, Lee E, Alt FW, Westphal H. 1996 Efficient in vivo manipulation of mouse genomic sequences at the zygote stage. Proc Natl Acad Sci U S A 93: 5860–5865. [PubMed: 8650183]

Lerner-Ellis JP, Tirone JC, Pawelek PD, Dore C, Atkinson JL, Watkins D, Morel CF, Fujiwara TM, Moras E, Hosack AR et al. 2006 Identification of the gene responsible for methylmalonic aciduria and homocystinuria, cblC type. Nat Genet 38: 93–100. [PubMed: 16311595]

Leung KY, Pai YJ, Chen Q, Santos C, Calvani E, Sudiwala S, Savery D, Ralser M, Gross SS, Copp AJ et al. 2017 Partitioning of One-Carbon Units in Folate and Methionine Metabolism Is Essential for Neural Tube Closure. Cell Rep 21: 1795–1808. [PubMed: 29141214]

Levy HL, Mudd SH, Schulman JD, Dreyfus PM, Abeles RH. 1970 A derangement in B12 metabolism associated with homocystinemia, cystathioninemia, hypomethioninemia and methylmalonic aciduria. Am J Med 48: 390–397. [PubMed: 5435651]

Lipton SA, Kim WK, Choi YB, Kumar S, D'Emilia DM, Rayudu PV, Arnelle DR, Stamler JS. 1997 Neurotoxicity associated with dual actions of homocysteine at the N-methyl-D-aspartate receptor. Proc Natl Acad Sci U S A 94: 5923–5928. [PubMed: 9159176]

Mellman IS, Youngdahl-Turner P, Willard HF, Rosenberg LE. 1977 Intracellular binding of radioactive hydroxocobalamin to cobalamin-dependent apoenzymes in rat liver. Proc Natl Acad Sci U S A 74: 916–920. [PubMed: 15258]

Miyazaki J, Takaki S, Araki K, Tashiro F, Tominaga A, Takatsu K, Yamamura K. 1989 Expression vector system based on the chicken beta-actin promoter directs efficient production of interleukin-5. Gene 79: 269–277. [PubMed: 2551778]

Moreno-Garcia MA, Pupavac M, Rosenblatt DS, Tremblay ML, Jerome-Majewska LA. 2014 The Mmachc gene is required for pre-implantation embryogenesis in the mouse. Mol Genet Metab 112: 198–204. [PubMed: 24889031]

Mudd SH, Levy HL, Abeles RH, Jennedy JP Jr. 1969 A derangement in B 12 metabolism leading to homocystinemia, cystathioninemia and methylmalonic aciduria. Biochem Biophys Res Commun 35: 121–126. [PubMed: 5779140]

Muto Y, Maeda T, Suzuki K, Kato T, Watanabe F, Kamiyama H, Saito M, Koizumi K, Miyaki Y, Konishi F et al. 2014 DNA methylation alterations of AXIN2 in serrated adenomas and colon carcinomas with microsatellite instability. BMC Cancer 14: 466. [PubMed: 24964857]

Obeid R, Herrmann W. 2006 Mechanisms of homocysteine neurotoxicity in neurodegenerative diseases with special reference to dementia. FEBS Lett 580: 2994–3005. [PubMed: 16697371]

Okun JG, Horster F, Farkas LM, Feyh P, Hinz A, Sauer S, Hoffmann GF, Unsicker K, Mayatepek E, Kolker S. 2002 Neurodegeneration in methylmalonic aciduria involves inhibition of complex II and the tricarboxylic acid cycle, and synergistically acting excitotoxicity. J Biol Chem 277: 14674–14680. [PubMed: 11847233]

Olney JW, Price MT, Salles KS, Labruyere J, Ryerson R, Mahan K, Frierdich G, Samson L. 1987 L-homocysteic acid: an endogenous excitotoxic ligand of the NMDA receptor. Brain Res Bull 19: 597–602. [PubMed: 2891418]

Patterson ES, Waller LE, Kroll KL. 2014 Geminin loss causes neural tube defects through disrupted progenitor specification and neuronal differentiation. Dev Biol 393: 44–56. [PubMed: 24995796]

Pfaffl MW. 2001 A new mathematical model for relative quantification in real-time RT-PCR. Nucleic Acids Res 29: e45. [PubMed: 11328886]

Plesa M, Kim J, Paquette SG, Gagnon H, Ng-Thow-Hing C, Gibbs BF, Hancock MA, Rosenblatt DS, Coulton JW. 2011 Interaction between MMACHC and MMADHC, two human proteins participating in intracellular vitamin B(1)(2) metabolism. Mol GenetMetab 102: 139–148.

Profitlich LE, Kirmse B, Wasserstein MP, Diaz GA, Srivastava S. 2009 High prevalence of structural heart disease in children with cblC-type methylmalonic aciduria and homocystinuria. Mol Genet Metab 98: 344–348. [PubMed: 19767224]

Quintana AM, Geiger EA, Achilly N, Rosenblatt DS, Maclean KN, Stabler SP, Artinger KB, Appel B, Shaikh TH. 2014 Hcfc1b, a zebrafish ortholog of HCFC1, regulates craniofacial development by modulating mmachc expression. Dev Biol 396: 94–106. [PubMed: 25281006]

Schimel AM, Mets MB. 2006 The natural history of retinal degeneration in association with cobalamin C (cbl C) disease. Ophthalmic Genet 27: 9–14. [PubMed: 16543196]

Scott JM. 1999 Folate and vitamin B12. Proc Nutr Soc 58: 441–448. [PubMed: 10466189]

Shaw GM, Vollset SE, Carmichael SL, Yang W, Finnell RH, Blom H, Ueland PM. 2009 Nested case-control study of one-carbon metabolites in mid-pregnancy and risks of cleft lip with and without cleft palate. Pediatr Res 66: 501–506. [PubMed: 19668105]

Sloan JL, Achilly NP, Arnold ML, Catlett JL, Blake T, Bishop K, Jones M, Harper U, English MA, Anderson S et al. 2020 The vitamin B12 processing enzyme, mmachc, is essential for zebrafish survival, growth and retinal morphology. Hum Mol Genet 29: 2109–2123. [PubMed: 32186706]

Steele JW, Kim SE, Finnell RH. 2020 One-carbon metabolism and folate transporter genes: Do they factor prominently in the genetic etiology of neural tube defects? Biochimie 173: 27–32. [PubMed: 32061804]

Stiefel D, Shibata T, Meuli M, Duffy PG, Copp AJ. 2003 Tethering of the spinal cord in mouse fetuses and neonates with spina bifida. J Neurosurg 99: 206–213.

Tanpaiboon P, Sloan JL, Callahan PF, McAreavey D, Hart PS, Lichter-Konecki U, Zand D, Venditti CP. 2013 Noncompaction of the ventricular myocardium and hydrops fetalis in cobalamin C disease. JIMD Rep 10: 33–38. [PubMed: 23430797]

Ting SB, Wilanowski T, Auden A, Hall M, Voss AK, Thomas T, Parekh V, Cunningham JM, Jane SM. 2003 Inositol- and folate-resistant neural tube defects in mice lacking the epithelial-specific factor Grhl-3. Nat Med 9: 1513–1519. [PubMed: 14608380]

Tomaske M, Bosk A, Heinemann MK, Sieverding L, Baumgartner ER, Fowler B, Trefz FK. 2001 CblC/D defect combined with haemodynamically highly relevant VSD. J Inherit Metab Dis 24: 511–512. [PubMed: 11596656]

Watkins D, Rosenblatt DS. 2013 Lessons in biology from patients with inborn errors of vitamin B12 metabolism. Biochimie 95: 1019–1022. [PubMed: 23402785]

Weisfeld-Adams JD, Morrissey MA, Kirmse BM, Salveson BR, Wasserstein MP, McGuire PJ, Sunny S, Cohen-Pfeffer JL, Yu C, Caggana M et al. 2010 Newborn screening and early biochemical follow-up in combined methylmalonic aciduria and homocystinuria, cblC type, and utility of methionine as a secondary screening analyte. Mol Genet Metab 99: 116–123. [PubMed: 19836982]

Wilson MP, Hugge C, Bielinska M, Nicholas P, Majerus PW, Wilson DB. 2009 Neural tube defects in mice with reduced levels of inositol 1,3,4-trisphosphate 5/6-kinase. Proc Natl Acad Sci U S A 106: 9831–9835. [PubMed: 19482943]

Highlights

New mouse models to study the role of cobalamin (vitamin B_{12}) metabolism in mammalian development

Mmachc loss results in a pleiotropic phenotype and midgestational embryonic lethality

Development of the eye, heart, neural tube, and craniofacial skeleton are severely compromised

An *Mmachc* floxed allele to determine the tissue-specific requirements of cobalamin metabolism

Transgenic expression of *Mmachc* is capable of a maternal-effect rescue of *Mmachc* mutant lethality

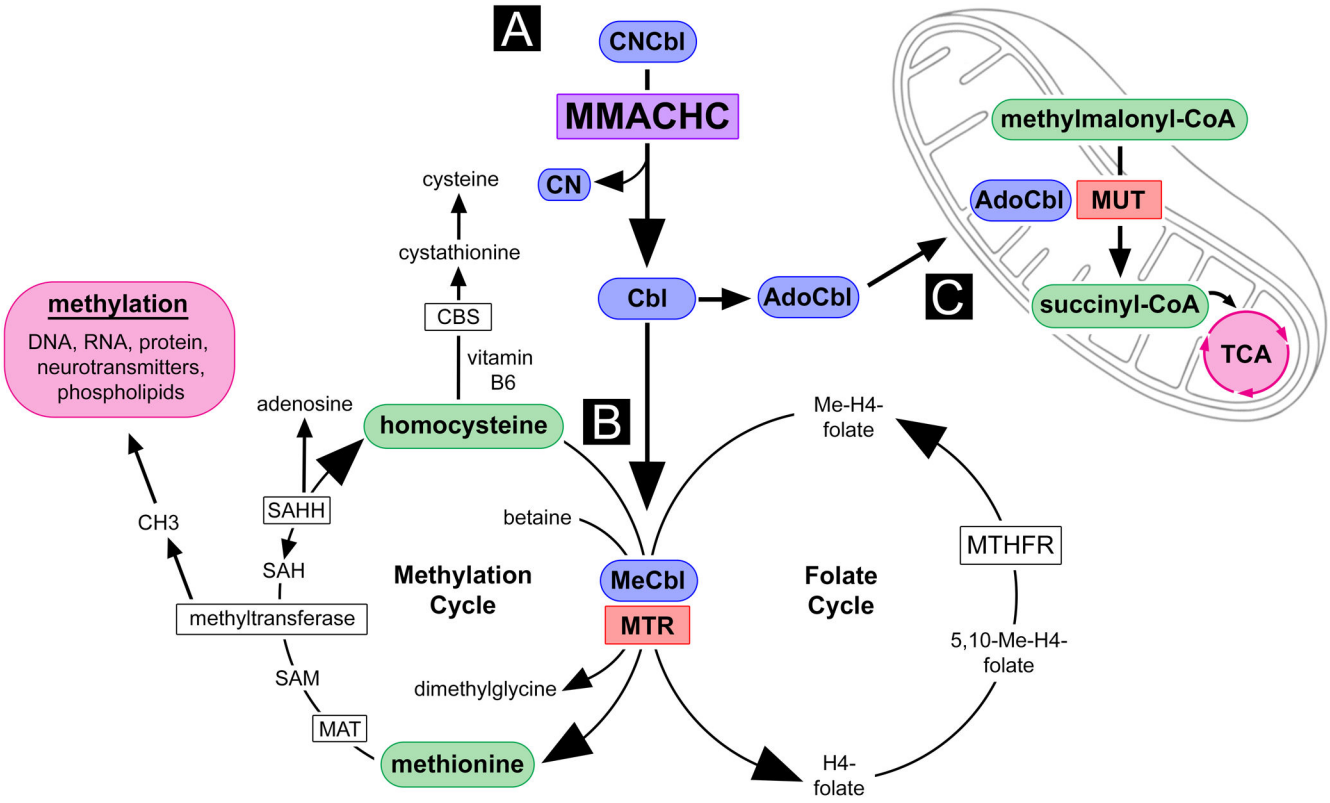

Figure 1. MMACHC-dependent metabolic pathways.

MMACHC converts dietary cobalamin from an inactive to active co-enzyme forms MeCbl and AdoCbl (A). The MeCbl co-enzyme functions in the cytoplasm with the enzyme MTR to convert homocysteine to methionine (B). The AdoCbl co-enzyme functions in the mitochondria with the enzyme MUT to convert methylmalonyl-CoA to the TCA cycle intermediate succinyl-CoA (C). See text for details.

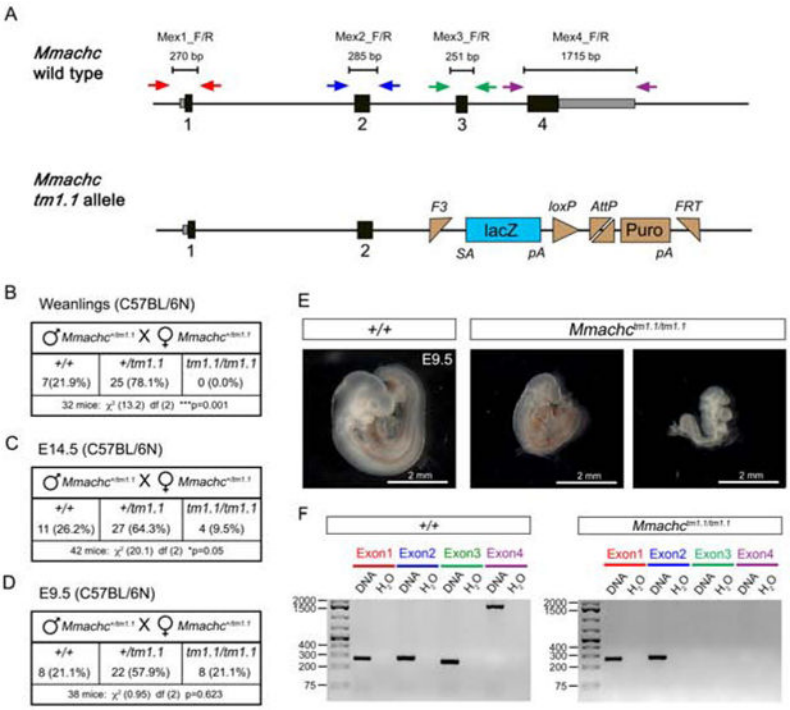

Figure 2. The *Mmachc tm1.1* allele is embryonic lethal.

Schematic of the wild-type and *tm1.1* alleles of *Mmachc* (A). *Mmachc*$^{+/tm1.1}$ intercrosses failed to produce viable *Mmachc*$^{tm1.1/tm1.1}$ offspring at weaning (B). Four *Mmachc*$^{tm1.1/tm1.1}$ mutants (9.5%) were recovered at E14.5 (C) and 8 (21.1%) were recovered at E9.5 (D). Images of E9.5 control and homozygous mutant embryos (E). PCR analysis of genomic DNA from these mutants (n = 3 per genotype) verified that exons 3 and 4 are deleted as expected (F).

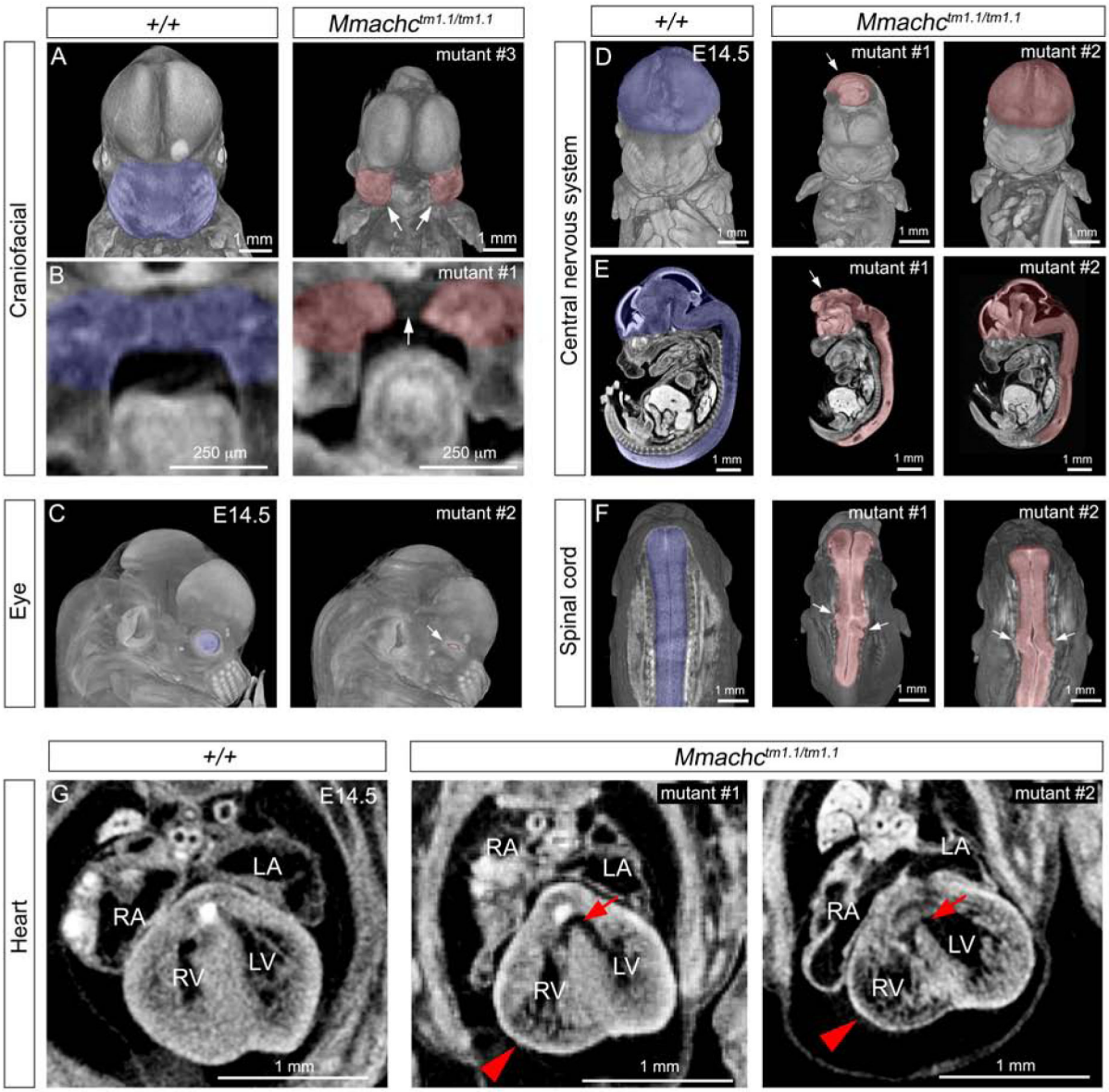

Figure 3. The *Mmachc tm1.1* allele impacts developing tissues often affected in cblC.

Micro-CT analysis of *Mmachc*$^{tm1.1/tm1.1}$ mutant embryos uncovered severe craniofacial defects including facial clefting (A) and a failure of palate fusion (B). *Mmachc*$^{tm1.1/tm1.1}$ mutants also showed microphthalmia (arrow in C) and anophthalmia (not shown). CNS defects include exencephaly (arrows in D), a wavy spinal cord (F), and thin, hypertrabeculated ventricles (arrowheads in G) and ventricular septum defects (arrows in G). n = 4 per genotype. RA = right atrium, LA = left atrium, RV = right ventricle, LV = left ventricle.

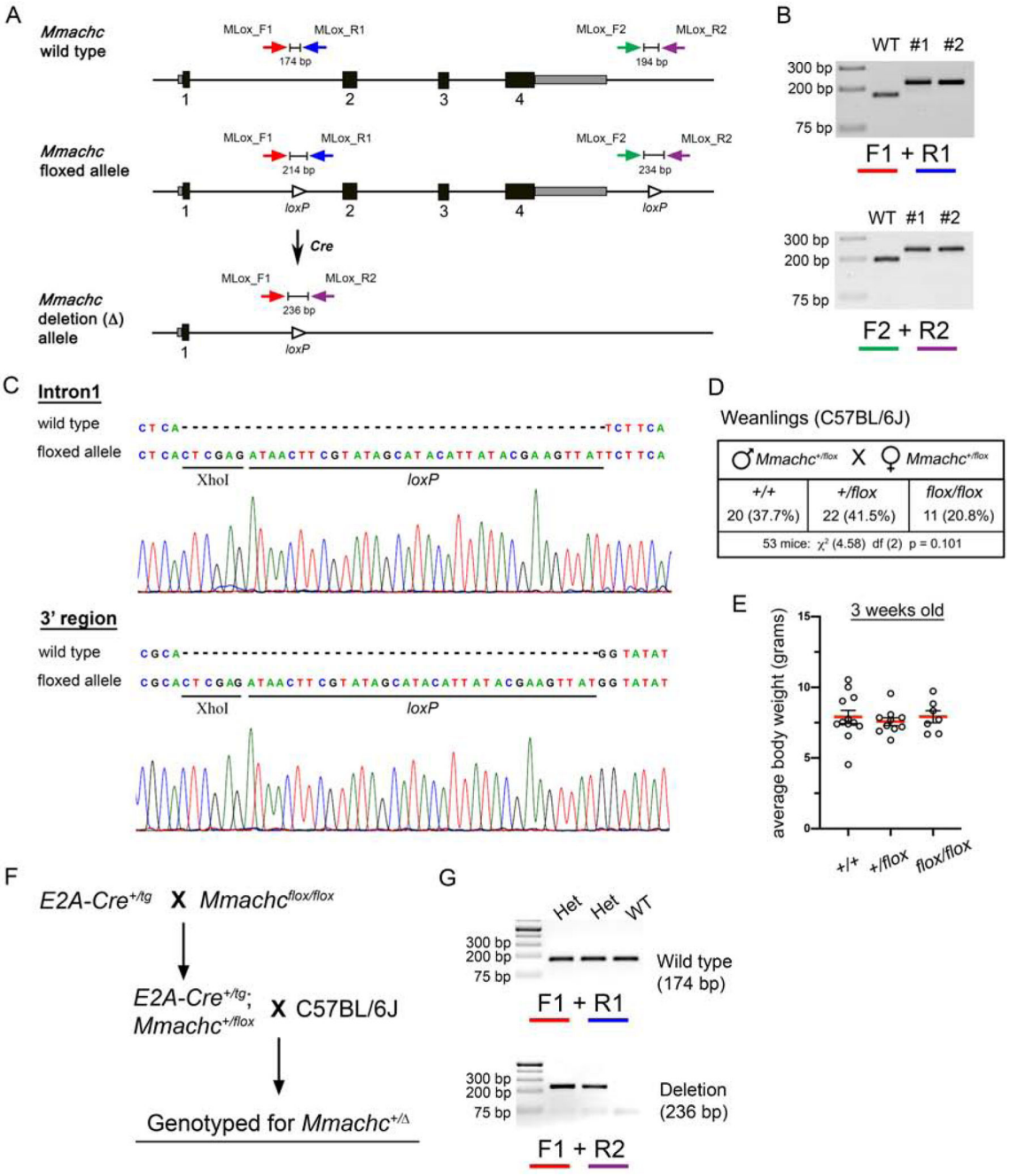

Figure 4. Generation and characterization of the *Mmachc* floxed allele.

Schematic of the wild-type, floxed, and Cre-mediated deletion allele of *Mmachc* (A). PCR genotyping of 2 founders showing homozygous targeting of both loxP sites . Sequencing of the targeted allele confirming loxP site insertion (C). *Mmachc*$^{+/flox}$ intercrosses showed that *Mmachc*$^{flox/flox}$ mice are born at normal Mendelian ratios, are viable, and do not exhibit any obvious phenotype (D-E). Crosses to the *E2A-Cre* deleter strain to generate germline *Mmachc* deletion mutants (F). PCR genotyping confirmed the generation of the deletion allele (G).

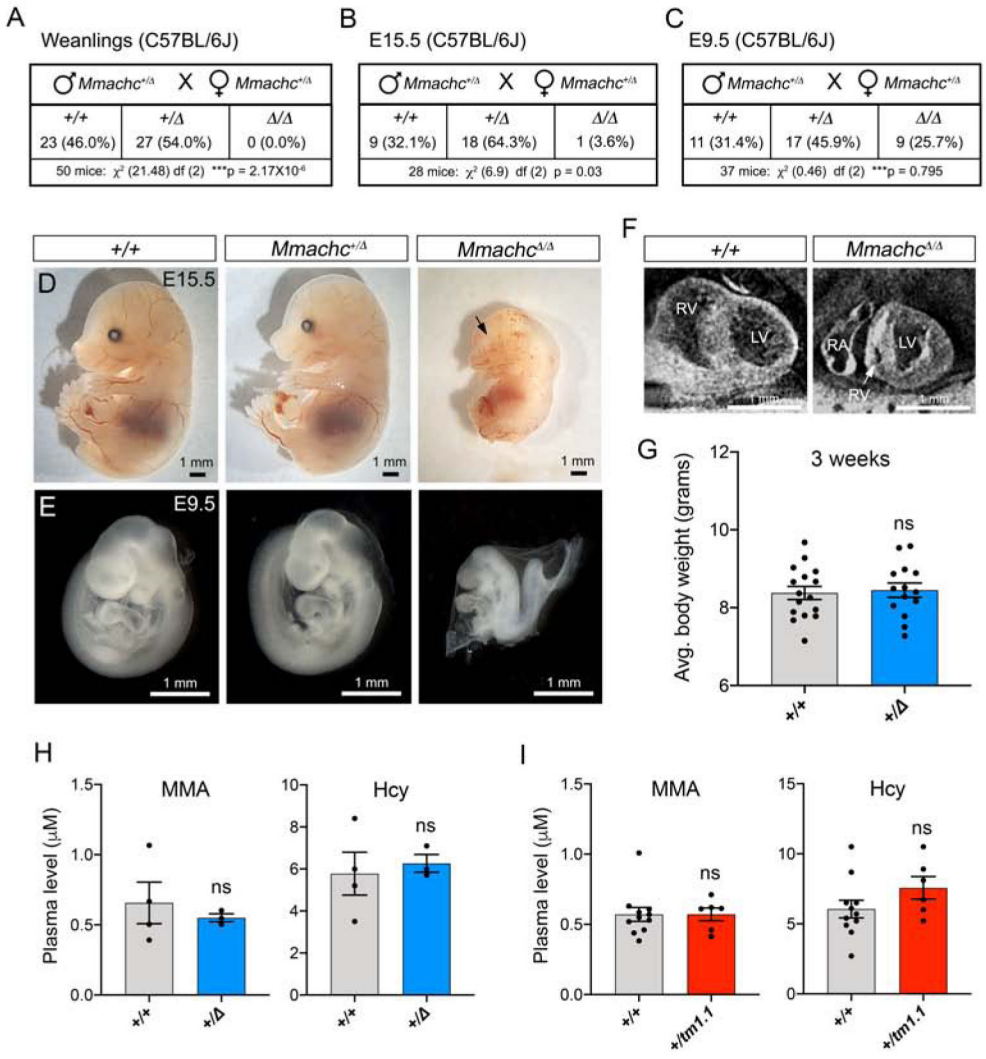

Figure 5. *Mmachc* deletion (Δ) allele is embryonic lethal.

Intercrosses of heterozygous deletion mutants (*Mmachc*$^{+/\Delta}$) failed to produce viable *Mmachc* $^{\Delta/\Delta}$ weanlings (A). E15.5 mutants were underrepresented (B), but E9.5 mutants were observed at normal Mendelian ratios (C). Microscopy revealed *Mmachc* mutant developmental defects (D-E). E14.5 *Mmachc*$^{\Delta/\Delta}$ heart exhibits right ventricular hypoplasia (arrow in F). Weight of wild-type and *Mmachc*$^{+/\Delta}$ mice (G). Adult *Mmachc* heterozygous mutant and wild-type plasma levels of MMA and Hcy (H-I). n > 3 per genotype.

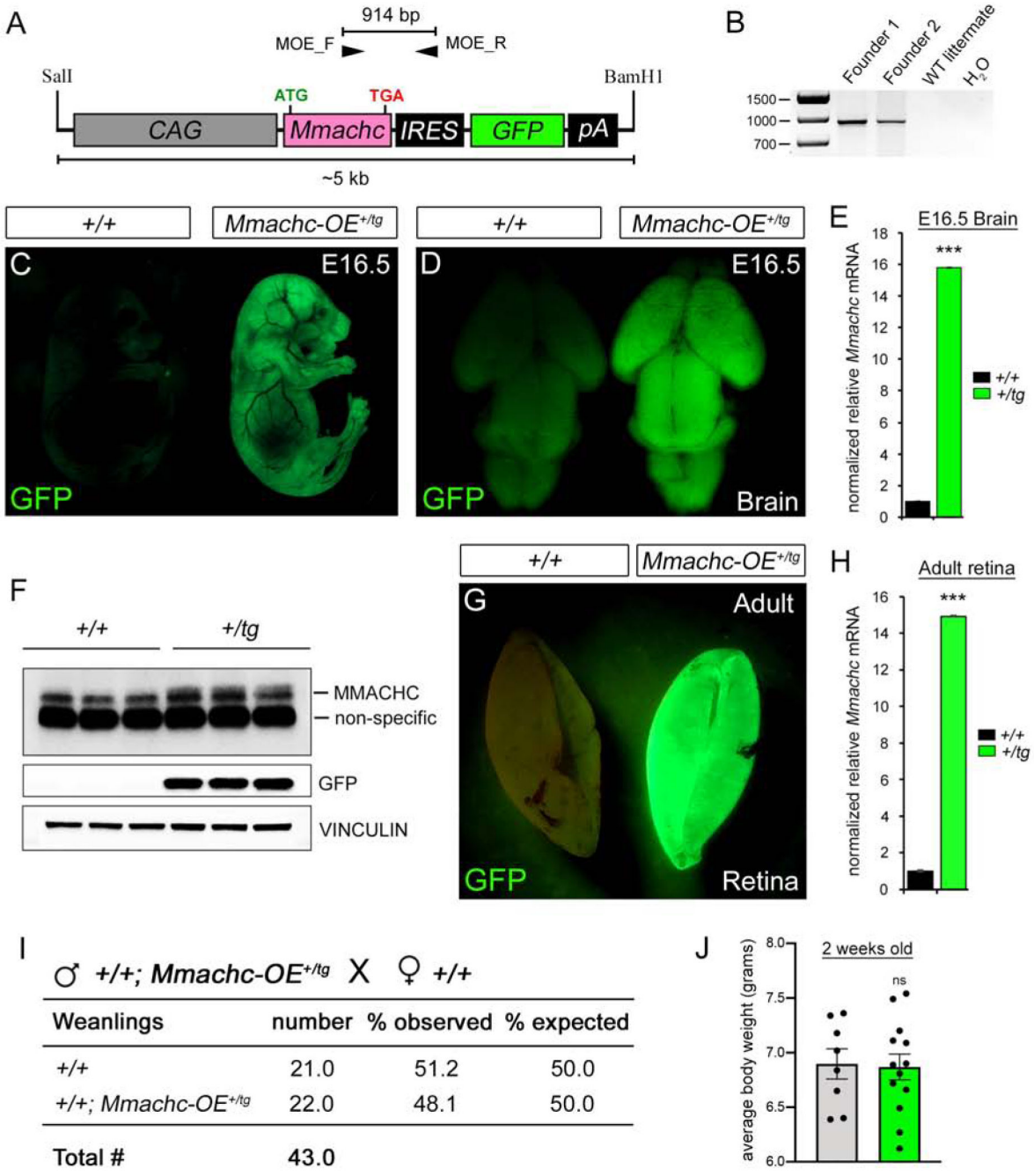

Weanlings	number	% observed	% expected
+/+	21.0	51.2	50.0
+/+; Mmachc-OE+/tg	22.0	48.1	50.0
Total #	43.0		

Figure 6. Generation and characterization of the *Mmachc-OE* transgenic mouse line.

Schematic of the transgenic DNA construct (A). Transgene-specific PCR genotyping of 2 founders (B). GFP fluorescence in E16.5 embryos (C) and brains (D). QrtPCR data showing increased *Mmachc* mRNA (E) and protein levels (F) relative to wild-type mice. GFP fluorescence in adult retinae (G) and qrtPCR data showing increased *Mmachc* mRNA (H). Crosses of *Mmachc-OE*$^{+/tg}$ to wild-type mice showed Mendelian inheritance of the transgene (I). Normal weight of *Mmachc-OE*$^{+/tg}$ weanlings (J). n ≥ 3 per genotype.

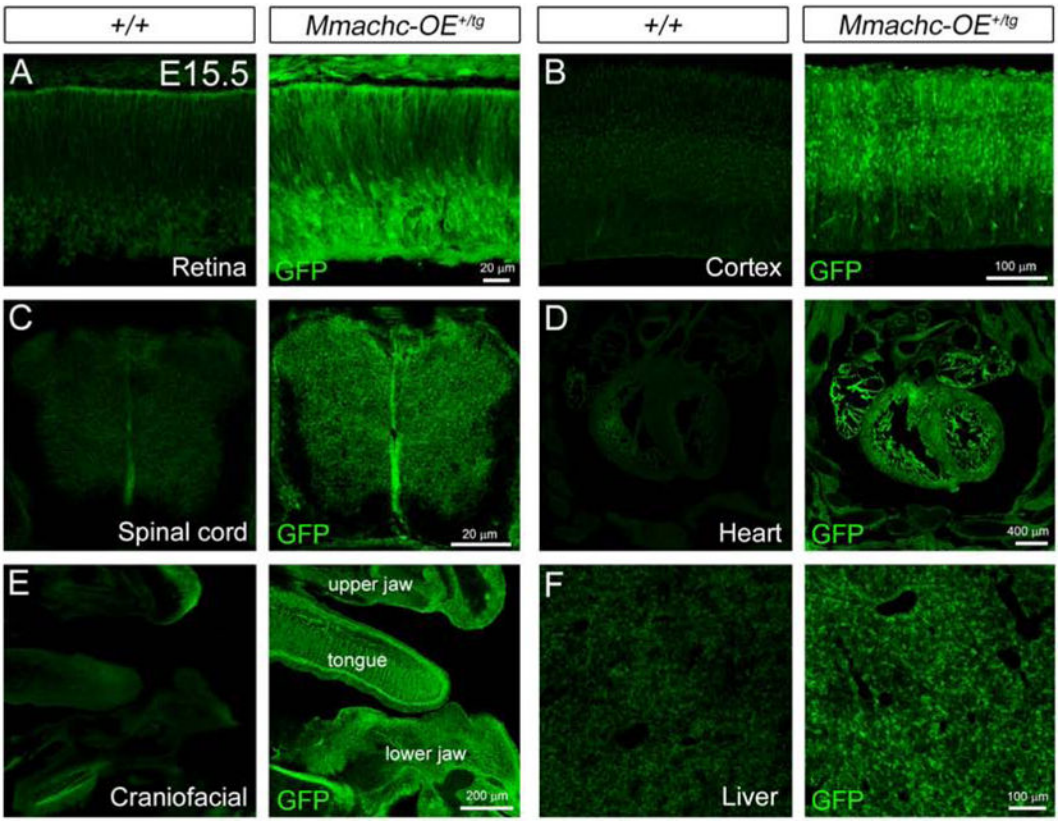

Figure 7. The *Mmachc-OE* transgene is expressed in developing tissues impacted by cblC.
GFP fluorescence in the E15.5 embryonic retina (A), cerebral cortex (B), spinal cord (C), heart (D), craniofacial region (E), and liver (F). n = 3 per genotype.

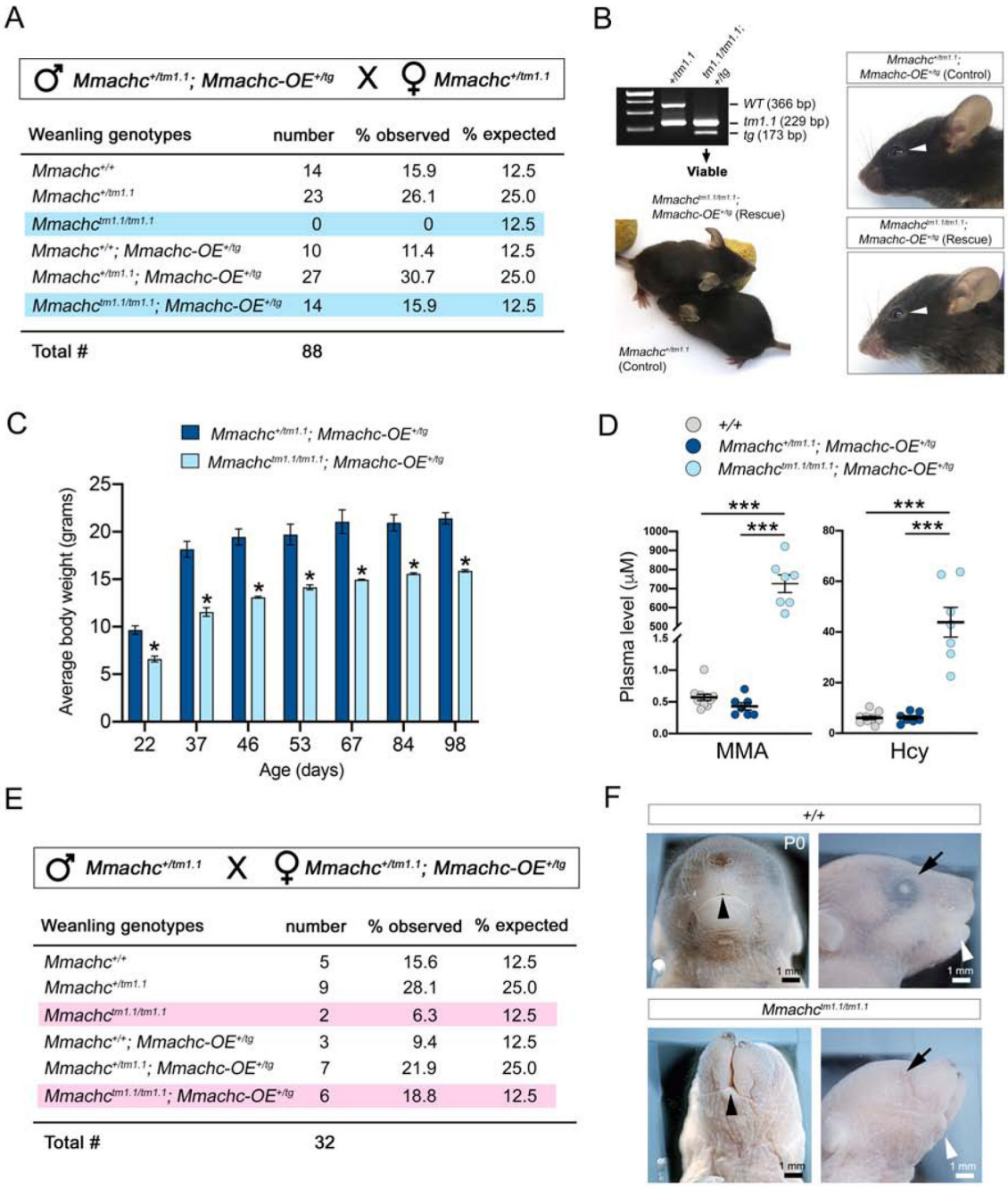

Figure 8. The *Mmachc-OE* transgene is functional *in vivo*.

Crosses showing that the *Mmachc-OE* transgene rescues the *Mmachc*$^{tm1.1/tm1.1}$ embryonic lethal phenotype (A). PCR genotyping and rescued *Mmachc*$^{tm1.1/tm1.1}$*; Mmachc-OE*$^{+/tg}$ weanling next to a littermate control (B). Ocular and craniofacial phenotypes appear fully rescued (B, arrowheads). *Mmachc*$^{tm1.1/tm1.1}$*; Mmachc-OE*$^{+/tg}$ mice are approximately 30% smaller than littermate controls (n =3 per genotype) (C). Adult *Mmachc*$^{tm1.1/tm1.1}$*; Mmachc-OE*$^{+/tg}$ and control plasma levels of MMA and Hcy (D). Crosses suggesting that the *Mmachc-OE* transgene is capable of a partially penetrant maternal-effect rescue resulting in viable offspring (E). Maternal-effect partial rescue of *Mmachc*$^{tm1.1/tm1.1}$ mutant lethality to

postnatal day 0 but showing a failure to rescue the eye and craniofacial phenotypes (F, arrows and arrowheads).